PERGAMON

International Journal of Solids and Structures 40 (2003) 3493–3505

INTERNATIONAL JOURNAL OF SOLIDS and STRUCTURES

www.elsevier.com/locate/ijsolstr

Ultrasonic scattering by a side-drilled hole

Anders Boström [a,*], Peter Bövik [b]

[a] *Department of Applied Mechanics, Division of Solid Mechanics, Chalmers University of Technology, Göteborg SE-412 96, Sweden*
[b] *Department of Mechanical Engineering, Chalmers Lindholmen University College, Box 8873, Göteborg SE-402 72, Sweden*

Received 26 June 2002; received in revised form 20 February 2003

Abstract

The scattering of elastic waves by a side-drilled hole (sdh) i.e. a circular cylindrical cavity, is considered. The scattering of plane or cylindrical waves by an sdh is an old subject; here the T matrix solution is adopted. The elastic waves are excited by an ultrasonic probe and a model of such a probe is thus used. The waves from the probes are expressed as a Fourier transform, i.e. as a superposition of plane waves. These plane waves are then transformed to the cylindrical system centred at the sdh. To obtain the signal in a receiving ultrasonic probe an electromechanical reciprocity relation is used. The signal response is obtained as a double wavenumber integral and an azimuthal summation. In the far field the integrals can be calculated approximately by the stationary phase approximation. Some numerical examples are given, in particular concentrating on when this approximation is valid.

Keywords: Wave propagation; Scattering; Ultrasonics; Side-drilled hole

1. Introduction

Ultrasonic nondestructive testing for defects is a common testing procedure in some applications, e.g. in aerospace, process, and nuclear power industries. To get a deeper understanding of the testing a mathematical modelling is very valuable and therefore many more or less sophisticated models have been developed through the years. A good model can be used for parametric studies much more easily than experimental work, and is therefore well suited for development of testing procedures and qualification of procedures and personnel.

In ultrasonic NDT calibration is performed by a side-drilled hole (sdh for short), a flat-bottomed hole or a notch. The sdh is probably the most well-defined and reproducible reflector and is therefore very well suited for this purpose. The scattering by an sdh is treated in the literature in a number of ways. Krautkrämer and Krautkrämer (1990) use simple high-frequency arguments to investigate the scattering dependence on frequency and sdh radius. Chapman (1990) uses the Kirchhoff approximation in conjunction with a simple model of an ultrasonic probe to determine the scattering by an sdh and employs this for

* Corresponding author. Tel.: +46-31-772-1500; fax: +46-31-772-3827.
E-mail address: anders.bostrom@me.chalmers.se (A. Boström).

0020-7683/03/$ - see front matter © 2003 Elsevier Science Ltd. All rights reserved.
doi:10.1016/S0020-7683(03)00150-1

calibration, see also Schmerr (1998). The Kirchhoff approximation is a high frequency method, but in this context it works well for ultrasonic wavelengths that are less than the sdh diameter. Purely numerical methods, like FEM (Harumi and Uchida, 1990) and EFIT (Fellinger et al., 1995; Halkjaer, 2000) are also in use, but are most useful in 2D as the number of unknowns often becomes too large in 3D.

As the sdh is a coordinate surface in cylindrical coordinates, the scattering problem can be solved analytically in terms of Bessel and Hankel functions. In 2D this solution was given long ago by White (1958), but only for plane wave incidence, see also Pao and Mow (1973) and Varadan et al. (1991). However, there seem to be no attempts to use the analytical solution in combination with realistic models of ultrasonic probes in transmission and reception. This is therefore the purpose of the present paper.

To model ultrasonic probes the approach of Boström and Wirdelius (1995) and Bövik and Boström (1997) is employed. This model replaces a transmitting probe by an effective traction boundary condition on the surface of the component where the probe is situated. A receiving probe is modelled with the help of a reciprocity result of Auld (1979). For the scattering by the sdh the null field solution as given by Olsson (1994) as part of a scattering problem in a pipe is employed. This solution is equivalent with the separation of variables solution, but it is convenient to employ the transition (T) matrix that results from the null field approach as this fully characterizes the sdh scattering for arbitrary incident fields.

2. The scattering problem

Consider the scattering by an sdh in an elastic half-space. The axis of the sdh is parallel with the surface of the half-space and is located at the depth d_z from this surface. The radius of the sdh is a. On the surface of the half-space two ultrasonic probes are located, one is acting as transmitter and the other as receiver. As a special case the transmitter may also act as a receiver.

Each probe has an attached coordinate system $x_t y_t z_t$ for the transmitter and $x_r y_r z_r$ for the receiver. The z_t and z_r axes are normal to the surface of the half-space, the x_t and x_r axes are normal to the sdh axis, and the y_t and y_r axes are parallel to the sdh axis. The xyz coordinate system is attached to the sdh with the origin in the $x_t z_t$ plane, the z axis as the sdh axis, the x axis parallel with the x_t and x_r axes, and the y axis antiparallel with the z_t and z_r axes. In the probe coordinate systems the vectors from the probes to the sdh are

$$\mathbf{d}_t = (d_{tx}, 0, -d_z) \tag{1}$$

$$\mathbf{d}_r = (d_{rx}, d_y, -d_z) \tag{2}$$

where d_y is the displacement between the probes in the axial direction of the sdh. In practice one usually takes $d_y = 0$.

The material of the half-space is assumed to be homogeneous, isotropic and linearly elastic with Lamé constants λ and μ and density ρ. Only time harmonic conditions with the time factor $\exp(-\mathrm{i}\omega t)$ is considered. The longitudinal and transverse wavenumbers are $k_p = \omega(\rho/(\lambda + 2\mu))^{1/2}$ and $k_s = \omega(\rho/\mu)^{1/2}$, respectively. The equation of motion for the displacement field is thus

$$k_p^{-2}\nabla(\nabla \cdot \mathbf{u}) - k_s^{-2}\nabla \times (\nabla \times \mathbf{u}) + \mathbf{u} = \mathbf{0} \tag{3}$$

which is written in a way which clearly indicates the decoupling into longitudinal and transverse waves.

The boundary condition on the sdh is that the surface traction vanishes there:

$$\mathbf{t}^{(\hat{r})} = \hat{\boldsymbol{r}} \cdot \boldsymbol{\sigma} = \hat{\boldsymbol{r}}\lambda\nabla \cdot \mathbf{u} + 2\mu\frac{\partial \mathbf{u}}{\partial r} + \mu\hat{\boldsymbol{r}} \times (\nabla \times \mathbf{u}) = 0 \tag{4}$$

where $\hat{\boldsymbol{r}}$ is the radial unit vector in the xy plane, r the corresponding radial coordinate and $\boldsymbol{\sigma}$ is the stress tensor.

On the planar surface of the half-space the traction vector

$$\mathbf{t}^{(\hat{z}_t)} = \hat{z}_t \cdot \boldsymbol{\sigma} = \hat{z}_t \lambda \nabla \cdot \mathbf{u} + 2\mu \frac{\partial \mathbf{u}}{\partial z_t} + \mu \hat{z}_t \times (\nabla \times \mathbf{u}) \tag{5}$$

where $\hat{z}_t = \hat{z}_r$ is the unit normal to the half-space, also vanishes except for the action of the probes. The transmitting probe is modelled by specifying the traction beneath the probe and the receiving probe is modelled by a reciprocity argument, see further in Sections 4 and 5, respectively.

The formulation of the scattering problem is completed by radiation conditions which in essence say that all energy is outward propagating far away from the probes. It is noted that a precise mathematical statement of the radiation conditions is not so easy in the present case which admits guided waves both along the free surface of the half-space (circular Rayleigh surface waves) and along the sdh. The surface waves along the sdh are also influenced by the presence of the planar free surface, this coupling being of significance only if the distance between the sdh and the planar surface is smaller than a few wavelengths.

To simplify the treatment all multiple scattering between the sdh and the surface of the half-space is neglected. This is justified if the distance d_z between the sdh and the surface of the half-space is a couple of wavelengths, particularly if it is noted that ultrasonic testing in practice is performed in the time domain where possible multiple scattering arrives later in time than the first stronger directly reflected wave.

3. The scattering by the sdh

To treat the scattering by the sdh it is clearly convenient to employ cylindrical coordinates $r\varphi z$ centred in the sdh, i.e. having the same origin as the xyz coordinate system. The scattering problem can then be solved by separation of variables in a straightforward way. However, here the null-field approach solution as given by Olsson (1994) is used as this is already available and is in a convenient format for the present purposes. It is noted that for the scattering by the sdh the null field approach yields the same exact solution as obtained by separation of variables.

To describe the scattering it is convenient to introduce the following set of cylindrical vector wave functions:

$$\begin{aligned}
\boldsymbol{\chi}^0_{1\sigma m}(h;\mathbf{r}) &= \sqrt{\frac{\varepsilon_m}{8\pi}} \frac{1}{q_s} \nabla \times \left[\hat{z} J_m(q_s r) \begin{pmatrix} \cos m\varphi \\ \sin m\varphi \end{pmatrix} \mathrm{e}^{\mathrm{i}hz} \right] \\
\boldsymbol{\chi}^0_{2\sigma m}(h;\mathbf{r}) &= \sqrt{\frac{\varepsilon_m}{8\pi}} \frac{i}{k_s q_s} \nabla \times \nabla \times \left[\hat{z} J_m(q_s r) \begin{pmatrix} \cos m\varphi \\ \sin m\varphi \end{pmatrix} \mathrm{e}^{\mathrm{i}hz} \right] \\
\boldsymbol{\chi}^0_{3\sigma m}(h;\mathbf{r}) &= \sqrt{\frac{\varepsilon_m}{8\pi}} \frac{1}{k_s} \nabla \left[J_m(q_p r) \begin{pmatrix} \cos m\varphi \\ \sin m\varphi \end{pmatrix} \mathrm{e}^{\mathrm{i}hz} \right]
\end{aligned} \tag{6}$$

Here J_m is a Bessel function and the Neumann factor is $\varepsilon_0 = 1$, $\varepsilon_m = 2$, $m = 1, 2, \ldots$ The axial wavenumber is h and the radial wavenumbers are $q_s = (k_s^2 - h^2)^{1/2}$ and $q_p = (k_p^2 - h^2)^{1/2}$, both with the branches defined so that $\mathrm{Im} q_s \geqslant 0$ and $\mathrm{Im} q_p \geqslant 0$. Real azimuthal functions are chosen and the index $\sigma = \mathrm{e}, \mathrm{o}$ (even, odd) determines the azimuthal parity. The first index τ (= 1, 2, 3) on the wave functions is the mode index with $\tau = 1$ for SH waves, $\tau = 2$ for SV waves and $\tau = 3$ for P waves. The normalizations are such that the wave

functions are dimensionless and give a simple Green tensor expansion. The superindex 0 on the wavefunctions indicates that they are regular for $r = 0$. The functions $\boldsymbol{\chi}^+$, which are defined with a Hankel function of the first kind instead of the Bessel function, give outward propagating waves and are also needed in the following. The functions $\tilde{\boldsymbol{\chi}}^0$ and $\tilde{\boldsymbol{\chi}}^+$ are defined with all explicit "i" in Eq. (6) changed to "−i".

The incoming field from the transmitting probe which is scattered by the sdh is treated in detail in the next section. At present it is enough to realize that the incoming field is regular in the vicinity of the sdh and thus admits a representation in terms of regular cylindrical waves:

$$\mathbf{u}^{\text{in}}(\mathbf{r}) = \sum_{\tau,\sigma,m} \int_{-\infty}^{\infty} \frac{\mathrm{d}h}{k_s} a_{\tau\sigma m}(h) \boldsymbol{\chi}^0_{\tau\sigma m}(h;\mathbf{r}) \tag{7}$$

Here the summations are over $\tau = 1, 2, 3$, $\sigma =$ e, o, and $m = 0, 1, 2, \ldots$ The expansion in Eq. (7) is valid in a cylinder circumscribing the sdh which just reaches the closest point of the transmitting probe.

The field scattered by the sdh also admits a representation in cylindrical waves, but this time the expansion is in terms of the outgoing waves:

$$\mathbf{u}^{\text{sc}}(\mathbf{r}) = \sum_{\tau,\sigma,m} \int_{-\infty}^{\infty} \frac{\mathrm{d}h}{k_s} f_{\tau\sigma m}(h) \boldsymbol{\chi}^+_{\tau\sigma m}(h;\mathbf{r}) \tag{8}$$

The unknown expansion coefficients $f_{\tau\sigma m}(h)$ can here be determined in terms of the known $a_{\tau\sigma m}(h)$ simply by using the traction free boundary condition on the sdh surface. As mentioned above, however, the null field solution by Olsson (1994) is employed. This solution yields the transition (T) matrix of the sdh, which is the matrix relating the expansion coefficients of the incoming field to those of the scattered field:

$$f_{\tau\sigma m}(h) = \sum_{\tau'} T^m_{\tau\sigma\tau'\sigma'}(h) a_{\tau'\sigma' m}(h) \tag{9}$$

As the sdh is a coordinate surface in the cylindrical coordinate system there is of course no coupling between different axial wavenumbers h and azimuthal orders m. The scattering by the sdh gives mode conversion so there is a coupling between different τ values. As opposed to the scattering by a sphere there is also mode coupling between the SH waves and the P and SV waves (except for $h = 0$ or $m = 0$). There is of course no coupling between different azimuthal parities, but a different σ' is still indicated in Eq. (9) because the $\tau\sigma$ indices decouple into the two groups $\tau\sigma =$ 1o, 2e, 3e (even parity) and $\tau\sigma =$ 1e, 2o, 3o (odd parity). The T matrices of the two groups are equal except that there is a sign change in the elements $\tau\tau' = 12, 21, 13, 31$ between the two groups.

All in all the T matrix can thus be viewed as a sum of two three by three matrices that only differ in some signs. Olsson (1994) gives explicit expressions for computing the T matrix. It is noted that the T matrix referred to the cylindrical waves as defined here is both symmetric and "hermitian" which can both be used as valuable checks on the computations.

4. The incoming field

To make a detailed modelling of a transmitting ultrasonic probe is a complicated matter. Here the common approach of modelling the probe by specifying the traction beneath it is used. The resulting boundary value problem with a specified traction on the surface of an elastic half-space can straightforwardly be solved by a double spatial Fourier transform. More details, such as the types of specified tractions that are possible, may be found in Boström and Wirdelius (1995).

Introduce the plane vector wave functions

$$\begin{aligned}
\boldsymbol{\phi}_1(\alpha,\beta;\mathbf{r}) &= \frac{1}{4\pi k_s \sin\alpha}\nabla\times(\hat{z}\mathrm{e}^{\mathrm{i}k_s\hat{\gamma}\cdot\mathbf{r}}) = -\frac{\mathrm{i}}{4\pi}\hat{\beta}\mathrm{e}^{\mathrm{i}k_s\hat{\gamma}\cdot\mathbf{r}}\\
\boldsymbol{\phi}_2(\alpha,\beta;\mathbf{r}) &= \frac{1}{4\pi k_s^2 \sin\alpha}\nabla\times\nabla\times(\hat{z}\mathrm{e}^{\mathrm{i}k_s\hat{\gamma}\cdot\mathbf{r}}) = -\frac{1}{4\pi}\hat{\alpha}\mathrm{e}^{\mathrm{i}k_s\hat{\gamma}\cdot\mathbf{r}}\\
\boldsymbol{\phi}_3(\alpha,\beta;\mathbf{r}) &= \left(\frac{k_p}{k_s}\right)^{3/2}\frac{1}{4\pi k_p}\nabla(\mathrm{e}^{\mathrm{i}k_p\hat{\gamma}\cdot\mathbf{r}}) = \left(\frac{k_p}{k_s}\right)^{3/2}\frac{\mathrm{i}}{4\pi}\hat{\gamma}\mathrm{e}^{\mathrm{i}k_p\hat{\gamma}\cdot\mathbf{r}}
\end{aligned} \tag{10}$$

Here the spherical unit vectors are

$$\begin{aligned}
\hat{\gamma} &= (\sin\alpha\cos\beta, \sin\alpha\sin\beta, \cos\alpha)\\
\hat{\alpha} &= (\cos\alpha\cos\beta, \cos\alpha\sin\beta, -\sin\alpha)\\
\hat{\beta} &= (-\sin\beta, \cos\beta, 0)
\end{aligned} \tag{11}$$

and α and β are the spherical angles of the direction of propagation of the plane wave. It is noted that α becomes complex for evanescent waves. The normalizations are such that the wave functions are dimensionless and give a simple Green tensor expansion. When discussing the transformation properties it is most natural to employ the variables α and β but from a computational point of view it is more convenient to employ the Fourier transform variables

$$\begin{aligned}
q &= k_j \sin\alpha\cos\beta\\
p &= k_j \sin\alpha\sin\beta
\end{aligned} \tag{12}$$

with $k_j = k_s$ or k_p as appropriate.

The field radiated by the transmitting probe can now be written

$$\mathbf{u}^{\mathrm{in}} = \sum_j \int_{-\infty}^{\infty}\int_{-\infty}^{\infty}\frac{\mathrm{d}q\,\mathrm{d}p}{k_j h_j}\xi_j(q,p)\boldsymbol{\phi}_j(\alpha,\beta;\mathbf{r}_t) \tag{13}$$

where $h_j = (k_j^2 - s^2)^{1/2}$ with $\mathrm{Im}h_j \geqslant 0$, $s = (q^2+p^2)^{1/2}$ and the summation is over $j = 1, 2, 3$. Expressions for the expansion coefficients ξ_j for various types of probes are given by Boström and Wirdelius (1995). As a simple example, for a specified traction that is constant (except for the phase) and only has a normal component:

$$\begin{aligned}
\xi_1(q,p) &= 0\\
\xi_2(q,p) &= A\frac{2\mathrm{i}k_s s h_s h_p}{R}T_z\\
\xi_3(q,p) &= -A\sqrt{k_p k_s}\frac{h_p(k_s^2 - 2s^2)}{R}T_z
\end{aligned} \tag{14}$$

where A is an amplitude factor. The Rayleigh function is

$$R = 4s^2 h_s h_p + (k_s^2 - 2s^2)^2 \tag{15}$$

and the double Fourier transform of the specified normal traction is

$$T_z = \frac{4k_s^2}{\pi Q p}\sin Qb\sin pc \tag{16}$$

Here

$$Q = q + k_i\sin\gamma \tag{17}$$

where γ is the angle of the probe and $k_i = k_s$ or k_p depending on the probe being of S or P type, respectively. The probe is assumed to be rectangular with sides b and c in the x_t and y_t directions, respectively, and the beam axis is assumed to lie in the $x_t z_t$ plane.

From a computational point of view it is natural to employ the Fourier variables q and p. When the expansion of the incoming field is going to be transformed to the cylindrical coordinates of the sdh, it is, however, more convenient to employ the angular variables α and β. Neglecting the evanescent waves the expansion Eq. (13) becomes

$$\mathbf{u}^{\text{in}} = \sum_j \int_{\pi/2}^{\pi} \sin\alpha \, \mathrm{d}\alpha \int_0^{2\pi} \mathrm{d}\beta \xi_j(q,p) \boldsymbol{\phi}_j(\alpha,\beta,\mathbf{r}_t) \tag{18}$$

where the relations between q and p and α and β are given in Eq. (12).

The transformation of Eq. (18) into an expansion in terms of the regular cylindrical waves of the sdh is performed in three steps. A translation followed by a rotation gives an expansion in plane waves in the xyz system and finally the plane waves are transformed to the cylindrical waves. Translation (which is trivial) and rotation with $-90°$ around the x axis gives

$$\mathbf{u}^{\text{in}} = \sum_{jj'} \int_0^{\pi} \sin\alpha' \, \mathrm{d}\alpha' \int_0^{\pi} \mathrm{d}\beta' \xi_j(q,p) \mathrm{e}^{\mathrm{i}k_j \hat{\gamma}\cdot\mathbf{d}_t} R_{jj'} \boldsymbol{\phi}_{j'}(\alpha',\beta',\mathbf{r}) \tag{19}$$

where the plane waves now are with respect to the xyz system. The relations between the spherical angles are

$$\begin{aligned} \sin\alpha\cos\beta &= \sin\alpha'\cos\beta' \\ \sin\alpha\sin\beta &= \cos\alpha' \\ \cos\alpha &= -\sin\alpha'\sin\beta' \end{aligned} \tag{20}$$

and the elements of the rotation matrix are

$$\begin{aligned} R_{11} &= R_{22} = \sin\beta\sin\beta' \\ R_{12} &= R_{21} = -\mathrm{i}\frac{\cos\beta'}{\sin\alpha} \\ R_{33} &= 1 \\ R_{13} &= R_{31} = R_{23} = R_{32} = 0 \end{aligned} \tag{21}$$

This form of the rotation matrix means that the SH and SV waves ($j = 1, 2$) are mixed by the rotation whereas the P wave ($j = 3$) is left unaffected.

The final step is the transformation to the cylindrical waves which is performed by the following

$$\boldsymbol{\phi}_\tau(\alpha',\beta',\mathbf{r}) = \frac{k_\tau}{k_s} \sum_{\sigma,m} D^{\dagger}_{\tau\sigma m}(\beta') \boldsymbol{\chi}^0_{\tau\sigma m}(k_\tau \cos\alpha';\mathbf{r}) \tag{22}$$

where

$$D^{\dagger}_{\tau\sigma m}(\beta') = \mathrm{i}^{m-\delta_{\tau 2}} \sqrt{\frac{\varepsilon_m k_s}{2\pi k_\tau}} \begin{pmatrix} \cos m\beta' \\ \sin m\beta' \end{pmatrix} \tag{23}$$

and the summation is over $\sigma = \mathrm{e}, \mathrm{o}$ and $m = 0, 1, 2, \ldots$ Insertion of Eq. (22) into Eq. (19) and changing the integration variable from α' to

$$h = k_\tau \cos\alpha' \tag{24}$$

then yields an expansion of the incoming field as in Eq. (7) with the expansion coefficients

$$a_{\tau\sigma m}(h) = \sum_j \int_0^\pi \mathrm{d}\beta' \xi_j(q,p) \mathrm{e}^{\mathrm{i}k_j\hat{\gamma}\cdot\mathbf{d}_t} R_{j\tau} D^{\dagger}_{\tau\sigma m}(\beta') \tag{25}$$

The transformations of variables that are needed in this equation are given in Eqs. (12), (20), and (24). As the evanescent waves have been neglected, Eq. (25) is only valid for propagating waves, i.e. for $|h| \leqslant k_\tau$. For $|h| > k_\tau$, $a_{\tau\sigma m}(h) = 0$.

5. The received signal response

So far the action of the transmitting probe and the scattering of the resulting field by the sdh have been treated. It now remains to determine the electrical signal of the receiving probe, this being the quantity that is measured in practice. To this end the electromechanical reciprocity result of Auld (1979) is ideal to use. Auld's result relates two different time harmonic elastodynamic states 1 and 2 generated by two different probes t and r (which as a special case may be the same). State 1 with displacement field $\mathbf{u}_1$ is due to an incident electric power P to probe t in the *presence* of the defect (the sdh in this case) and state 2 with displacement field $\mathbf{u}_2$ is due to incident electric power P to probe r in the *absence* of the defect. With these conditions Auld's result is

$$\delta\Gamma = -\frac{\mathrm{i}\omega}{4P} \int_S (\mathbf{u}_2 \cdot \mathbf{t}_1 - \mathbf{u}_1 \cdot \mathbf{t}_2)\, \mathrm{d}S \tag{26}$$

where $\delta\Gamma$ is the change in the electric reflection coefficient of probe r due to the presence of the defect, i.e. more or less the quantity measured in practice. The surface S is any control surface enclosing the defect and $\mathbf{t}_1$ and $\mathbf{t}_2$ are the surface tractions of state 1 and 2, respectively.

Now let state 1 be the actual situation of interest with the sdh and probe t acting as transmitter. The auxiliary state 2 has probe r as transmitter. The surface S can be the surface of the sdh although this is not necessary. In the vicinity of the sdh state 1 can be expanded as

$$\mathbf{u}_1 = \sum_{\tau,\sigma,m} \int_{-\infty}^{\infty} \frac{\mathrm{d}h}{k_s} \left[a^{(t)}_{\tau\sigma m}(h) \boldsymbol{\chi}^0_{\tau\sigma m}(h;\mathbf{r}) + f^{(t)}_{\tau\sigma m}(h) \boldsymbol{\chi}^+_{\tau\sigma m}(h;\mathbf{r}) \right] \tag{27}$$

which is just the sum of Eqs. (7) and (8) with a superscript t added to indicate the transmitting probe. State 2 can likewise be expanded as

$$\mathbf{u}_2 = \sum_{\tau,\sigma,m} \int_{-\infty}^{\infty} \frac{\mathrm{d}h}{k_s} \tilde{a}^{(r)}_{\tau\sigma m}(h) \tilde{\boldsymbol{\chi}}^0_{\tau\sigma m}(h;\mathbf{r}) \tag{28}$$

For a reason soon apparent the expansion is here performed with the wave functions with a tilde. Remember that this tilde means that all explicit "i" in the definition is changed to "−i". Equivalently this can be performed by changing "h" to "$-h$" and changing sign on the $\tau = 2$ wave function. This means that $\tilde{\boldsymbol{a}}^{(r)}$ can be determined from $a^{(r)}$ in the same manner.

When the expansions Eqs. (27) and (28) are inserted into Eq. (26) the resulting integrals over S can be computed using the Betti identities for cylindrical waves (which can be derived in the same manner as the spherical counterparts, see Pao (1979)):

$$\int_S \left[\tilde{\boldsymbol{\chi}}^0_{\tau'\sigma'm'}(h';\mathbf{r}) \cdot \mathbf{t}(\boldsymbol{\chi}^+_{\tau\sigma m}(h;\mathbf{r})) - \mathbf{t}(\tilde{\boldsymbol{\chi}}^0_{\tau'\sigma'm'}(h';\mathbf{r})) \cdot \boldsymbol{\chi}^+_{\tau\sigma m}(h;\mathbf{r}) \right] \mathrm{d}S = \mathrm{i}\mu\delta_{\tau\tau'}\delta_{\sigma\sigma'}\delta_{mm'}\delta(h-h') \tag{29}$$

$$\int_S \left[\tilde{\boldsymbol{\chi}}^0_{\tau'\sigma'm'}(h';\mathbf{r}) \cdot \mathbf{t}(\boldsymbol{\chi}^0_{\tau\sigma m}(h;\mathbf{r})) - \mathbf{t}(\tilde{\boldsymbol{\chi}}^0_{\tau'\sigma'm'}(h';\mathbf{r})) \cdot \boldsymbol{\chi}^0_{\tau\sigma m}(h;\mathbf{r}) \right] \mathrm{d}S = 0 \tag{30}$$

Here $\mathbf{t}$ denotes the surface traction operator, i.e. when S coincides with the surface of the sdh it is the operator defined through Eq. (4). The result for the signal response finally becomes

$$\delta\Gamma = \frac{\mu c_s}{4P} \sum_{\tau,\sigma,m} \int_{-k_\tau}^{k_\tau} \frac{\mathrm{d}h}{k_s} f^{(t)}_{\tau\sigma m}(h) \tilde{a}^{(r)}_{\tau\sigma m}(h) \tag{31}$$

Using also Eq. (9) this can be rewritten as

$$\delta\Gamma = \frac{\mu c_s}{4P} \sum_{\sigma,m} \sum_{\tau,\tau'} \int_{-k_{\tau\tau'}}^{k_{\tau\tau'}} \frac{\mathrm{d}h}{k_s} \tilde{a}^{(r)}_{\tau\sigma m}(h) T^m_{\tau\sigma\tau'\sigma'}(h) a^{(t)}_{\tau'\sigma' m}(h) \tag{32}$$

Here the integration limit is $k_{\tau\tau'} = \min(k_\tau, k_{\tau'})$ and the way to choose σ' was explained below Eq. (9). In Eq. (32) the effects of the transmitting probe (given by $a^{(t)}$), the sdh (given by T) and the receiving probe (given by $\tilde{a}^{(r)}$) are clearly separated in a very nice fashion, cf. Boström and Wirdelius (1995) for the corresponding result for spherical waves.

6. Far field approximations

As the signal response as derived in Eq. (32) contains a double integral (note that the expansion coefficient of the incoming field in Eq. (25) contains an integral) it is computationally rather demanding if time domain results which also include a frequency integration are asked for. Therefore, it is of interest to investigate approximate calculations of the integrals. This also has the advantage of leading to results that are more easy to interpret.

The most obvious way of approximating the integrals is by using the stationary phase approximation with the distance between the probe and the sdh as the large parameter. The approximation is performed in two steps: first the β' integral in the expansion coefficients of the incoming field in Eq. (25) is calculated and then the h integral in the signal response in Eq. (32). The exponent in the integrand in Eq. (25) can be written

$$k_j \hat{\boldsymbol{\gamma}} \cdot \mathbf{d}_t = k_j d_t \sin\alpha \sin(\beta' - \varphi_t) \tag{33}$$

where $d_t = (d_{tx}^2 + d_z^2)^{1/2}$ is the distance between the transmitter and the sdh and φ_t is the angle between $\mathbf{d}_t$ and the negative z_t exist. The large parameter in the stationary phase approximation is $k_j d_t \sin\alpha$ and the only stationary point appears at $\beta' = \varphi_t + \pi/2$ (note that $0 \leqslant \beta' \leqslant \pi$ and $-\pi/2 < \varphi_t < \pi/2$). With this it is easy to obtain the approximation

$$a_{\tau\sigma m}(h) = \sqrt{\frac{2\pi}{k_\tau d_t \sin\alpha}}\ \mathrm{e}^{\mathrm{i}(k_\tau d_t \sin\alpha - \pi/4)} \sum_j \xi_j(q,p) R_{j\tau} D^{\dagger}_{\tau\sigma m}(\beta') \Big|_{\beta' = \varphi_t + \pi/2} \tag{34}$$

where the effects of fixing β' on the other parameters are determined by Eqs. (12) and (20).

For the h integral in Eq. (32) the phase function comes from the exponent in Eq. (34) from the transmitting probe and a similar contribution from the receiving probe

$$\psi(h) = d_t \sqrt{k_\tau^2 - h^2} + d_r \sqrt{k_{\tau'}^2 - h^2} - d_y h \tag{35}$$

where $d_r = (d_{rx}^2 + d_z^2)^{1/2}$. The last term appears because the receiving probe is located at $y = d_y$ and not at $y = 0$ as the transmitting one. The minus sign is due to the tilde on $a^{(r)}$ in Eq. (32) as explained earlier. When $d_y = 0$ the stationary point of ψ is at $h = 0$ and when $k_\tau = k_{\tau'}$ it is at $h = k_\tau d_y / ((d_r + d_t)^2 + d_y^2)^{1/2}$. When $d_y \neq 0$ and $k_\tau \neq k_{\tau'}$ no simple analytical solution for the stationary point can be obtained but it can of course be obtained numerically in a straightforward way.

The stationary phase approximation of Eq. (32) then becomes

$$\delta\Gamma = \frac{\mu c_s}{4P}\sum_{\tau,\tau'}\frac{2\pi}{k_s\sqrt{d_t d_r\sqrt{(k_\tau^2-h^2)(k_{\tau'}^2-h^2)}}}\sqrt{\frac{2\pi}{|\psi''(h)|}}\ \mathrm{e}^{\mathrm{i}(\psi(h)-3\pi/4)} \times \sum_{\sigma,m} T^m_{\tau\sigma\tau'\sigma'}\left[\sum_j \xi_j^{(t)}(q_t,h)R_{j\tau}D^{\dagger}_{\tau\sigma m}(\beta'_t)\right]_{\beta'_t=-\sqrt{k_\tau^2-h^2}\sin\varphi_t} \times \left[(-1)^{\delta_{\tau'2}}\sum_{j'}\xi_{j'}^{(r)}(q_r,-h)R_{j'\tau'}D^{\dagger}_{\tau'\sigma' m}(\beta'_r)\right]_{\beta'_r=-\sqrt{k_{\tau'}^2-h^2}\sin\varphi_r} \tag{36}$$

where the stationary value for h should be inserted and indices t and r have been inserted to distinguish quantities referring to the transmitting and receiving probe, respectively.

As it stands Eq. (36) is a little formal and not very illuminating, although it is straightforward to compute numerically.

To gain a better understanding two special cases are now considered. First assume that the two probes are both primarily emitting P waves. Neglecting all S waves (i.e. put $\xi_1 = \xi_2 = 0$) gives in a straightforward way the more explicit expression

$$\delta\Gamma_{PP} = \frac{\mu c_s}{4\pi}\sqrt{\frac{2\pi}{k_p^3 d_t d_r d}}\ \mathrm{e}^{\mathrm{i}(k_p d-3\pi/4)}\xi_3^{(t)}(q_t,h)\xi_3^{(r)}(q_r,-h)\sum_m \varepsilon_m(-1)^m T^m_{33}(h)\cos m(\varphi_t-\varphi_r) \tag{37}$$

where $d = ((d_t+d_r)^2+d_y^2)^{1/2}$ is the distance between transmitter and receiver along the ray reflected at the sdh axis and the stationary values $h = k_p d_y/d$ and $q_i = -(k_p^2-h^2)^{1/2}\sin\varphi_i$, $i = t, r$, should be inserted. The σ indices on T^m_{33} have been suppressed as $T^m_{3e3e} = T^m_{3o3o} = T^m_{33}$. The phase dependence on distance through the factor $k_p d$ in the exponential is the one expected from ray physics. When d_t is of the same order as d_r the amplitude dependence on distance is $d^{-3/2}$ which is expected as the transmitter gives a factor d^{-1} and the sdh scattering a factor $d^{-1/2}$ (as this scattering is in essence two dimensional).

As a second example consider an S probe acting in pulse-echo, i.e. the transmitter also acts as receiver. Then assume $\xi_3 = 0$. The stationary point is at $h = 0$ and the stationary value $\beta' = \varphi + \pi/2$ easily translates into $q = -k_s\sin\varphi_t$ and $p = 0$. The rotation matrix elements become $R_{11} = R_{22} = 0$ and $R_{12} = R_{21} = \mathrm{i}$ which finally gives

$$\delta\Gamma_{ss} = \frac{\mu c_s}{4\pi}\frac{\mathrm{e}^{\mathrm{i}(2k_s d_t+\pi/4)}}{(k_s d_t)^{3/2}}\sqrt{\pi}\sum_m \varepsilon_m(-1)^m\left[(\xi_2(-k_s\sin\varphi_t,0))^2 T^m_{11}(0)+(\xi_1(-k_s\sin\varphi_t,0))^2 T^m_{22}(0)\right] \tag{38}$$

Note that there is no coupling between the SV and SH waves (no term $\xi_1\xi_2 T^m_{12}$). This easily follows from symmetry considerations. Depending on the probe being of SV or SH type only one of the terms in Eq. (38) is usually of importance. An example where both terms are important is for a rotated SV probe, for which the beam axis is not in the $x_t z_t$ plane and ξ_1 and ξ_2 are of about equal size.

It is here worthwhile to a little closer examine when the stationary phase approximation leading to Eqs. (36)–(38) is expected to be valid. First the parameter in the exponent (essentially $k_j d$) should be large. Thus the distance between the probe and the sdh should be a couple of wavelengths, a condition usually met in practice. Next the rest of the integrands should be slowly varying functions of β' and h. This in particular means that the factors $\sin Qb$ and $\sin pc$ in Eq. (16) (which is only valid for a rectangular piston-like probe; a similar behaviour appears for other probes) must vary slowly which is only true if the probe near-field length $R = D^2/4\lambda_j$ (with D the probe diameter and λ_j the ultrasonic wavelength) is much smaller than the distance d_t between the probe and the sdh. This condition is often not satisfied in practice. Also the T matrix

$T^m(h)$ must be slowly varying as a function of h. This is not expected to be a trouble in practice. Note that the stationary phase approximation only approximates the axial scattering by the sdh and not the azimuthal scattering.

A way to avoid the restriction that the sdh should lie well outside the near-field length of the probe is to subdivide the probe into a number of elements. A natural strategy is to subdivide the probe into rectangular, almost quadratic, elements so that the near-field length of each element is much smaller than the distance between transmitter and sdh. The subdivision also has the merit that every element can be controlled separately, thus enabling the modelling of phased arrays and focused probes. For elliptic or irregular shaped probes the rectangular elements do not match the boundary very well, but this is of minor importance because the exact amplitude distribution across the probe is not crucial and is anyway not known in detail in practice. A drawback with subdividing the probe is that the stationary phase approximations contain an additional double sum over the elements of the transmitting and receiving probes, thus very quickly increasing the computational effort with the number of elements.

7. Numerical results

Turning to numerical examples, the difference between the direct integration in Eq. (32) and the stationary phase approximation in Eq. (36) (or Eq. (37) or (38) in special cases) will be illustrated. Only results with a fixed frequency are considered as this gives a well-defined wavelength and probe near-field length, two quantities that are important when the validity of the stationary phase approximation is investigated. The material of the component with the sdh is assumed to be steel with wave speeds $c_p = 5940$ m/s and $c_s = 3230$ m/s.

The computations are rather straightforward, but a few comments may be in order. The signal response for both the direct integration and the stationary phase approximation contains an azimuthal sum over m. To get convergence it is enough to take terms up to approximately $m_{\max} = [k_s a] + 10$ ($[\cdot]$ denotes the integer part). The integration over the axial wavenumbers in the signal response in Eq. (32) has been performed with 100 points in a Gauss–Legendre quadrature. This gives good accuracy for the present computations, but the number of points is somewhat dependent on the distance between the probe and sdh, increasing with distance due to the more oscillatory behaviour of the integrand.

In Table 1 the exact and approximate signal responses from an sdh with 2 mm radius at various depths are compared. The probe is a 0° P probe with frequency 2 MHz and side 1 mm (and the probe model used is such that all S waves are completely suppressed). This probe is unrealistically small but is chosen here because its near-field length is less than 1 mm and the only condition of importance for the validity of the stationary phase approximation is that the wavelength, which is almost 3 mm, should be smaller than the depth of the sdh. The results are calibrated against the exact result at depth $d = 40$ mm. As seen from the table the stationary phase approximation performs well, even at depth $d = 10$ mm (about three

Table 1
Exact and approximate signal responses for various depths of an sdh with radius 2 mm

d (mm)	Exact signal (dB)	Appr. signal (dB)
5	26.6	30.5
10	19.4	17.7
20	9.5	8.7
40	0.0	−0.4

0° P probe with side 1 mm, frequency 2 MHz and near field length less than 1 mm.

wavelengths) the discrepancy is only 1.7 dB. At depth $d = 5$ mm (one wavelength between the probe and the top of the sdh) the difference is 3.9 dB which is of course too much to be useful.

In Table 2 the situation is the same except that the probe size is changed to 20 mm, which is a typical size used in practice. The results are calibrated against the exact result at depth $d = 130$ mm. The near field length of this probe is 34 mm and as seen from the table the results for smaller depths than this are very far off. To get a really good result within 1 dB the depth has to be at least 130 mm, i.e. almost four near field lengths.

As stated in the previous section the validity of the stationary phase approximation requires that the distance between the probe and the sdh is much larger than the ultrasonic wavelength and the probe near-field length. The results from Tables 1 and 2 now make it possible to quantify this a little closer. For an accuracy of 1 dB the distance between the probe and sdh should be at least five times both the wavelength and the near-field length. Although no further results are given here, this statement is in fact more or less generally valid also for other probe sizes, types, and distances. It is in particular noted that the validity of the stationary phase approximation is more or less independent of the sdh radius (because the approximation only involves the axial scattering whereas the azimuthal sum is unaffected).

Another aspect of the scattering by an sdh is considered in Table 3 which shows the behaviour when the sdh radius is varied. The depth of the sdh is 50 mm and the probe has side 10 mm and frequency 1 MHz. The probe is thus operating in the far field and the results are obtained with the stationary phase approximation (but an exact integration would only differ very little). The left column shows results for a 0° P probe and the right column for a 45° SV probe. According to some simple arguments (Krautkrämer and Krautkrämer, 1990) the scattering by an sdh should increase with the square root of the radius. A doubling of the radius should thus lead to an increase in the received signal by $20 \log \sqrt{2} = 3.01$ dB. For the P probe in Table 3 this is seen to be very well satisfied for radii above 2 mm. That the simple rule breaks down for smaller radii is not surprising as the arguments behind the rule are of a high frequency nature which are

Table 2
Exact and approximate signal response for various depths of an sdh with radius 2 mm

d (mm)	Exact signal (dB)	Appr. signal (dB)
10	4.9	34.3
30	4.7	20.0
50	7.0	13.3
70	5.7	8.9
90	3.7	5.7
110	1.8	3.1
130	0.0	0.9

0° P probe with side 20 mm, frequency 2 MHz and near field length 34 mm.

Table 3
Signal response for an sdh of various radii and depth 50 mm

d (mm)	Signal P (dB)	Signal SV (dB)
0.25	−21.5	−15.8
0.5	−9.5	−4.6
1	0.0	0.0
2	2.2	1.1
4	5.2	3.2
8	8.3	6.6
16	11.4	11.6

Probe with side 10 mm and frequency 1 MHz and 0° probe in left column and 45° SVprobe in right column.

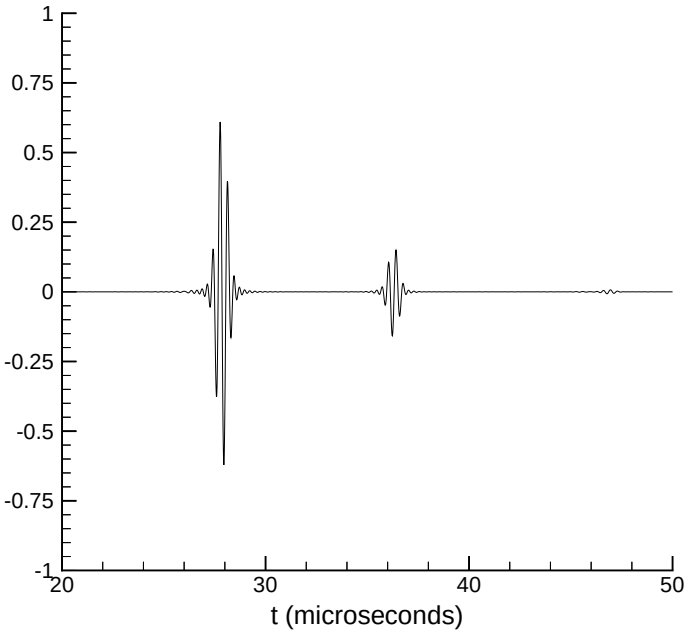

Fig. 1. The signal response as a function of time for an sdh with diameter 10 mm and centre depth 50 mm. 0° SV probe with side 2 mm and centre frequency 2 MHz.

definitely invalid for holes with diameter less than a wavelength. As seen from Table 3 the angled SV probe do not follow the rule very well, but why this is so is unclear.

As a last example Fig. 1 shows the signal response as a function of time. The sdh has a diameter of 10 mm and its centre depth is 50 mm. The probe is a 0° SV probe with centre frequency 2 MHz and a 100% Hanning window (meaning that the frequency content has a $\cos^2$ distribution with the peak at 2 MHz and zeroes at 0 ad 4 MHz). 200 equidistant frequencies have been employed, but 100 points give an almost identical result. The probe is square with side 2 mm. This is a smaller probe than used in real applications, but it is chosen because it gives a strong "creeping wave" response. The signal around $t = 28$ μs in Fig. 1 is the directly reflected SV wave (the probe is chosen to only generate and detect SV waves; a real probe of this size would also generate P waves and these can also be included in the model as explained in previous sections). The second signal around $t = 36$ μs is the creeping wave, its arrival time fits exactly with an SV wave hitting the sdh tangentially, then travelling around the back half of the sdh as a Rayleigh-like surface wave, and finally going back to the probe as an SV wave again. There is even a third, small signal at time $t = 47$ μs in Fig. 1 and this is the contribution from the creeping wave that has travelled one and a half way around the sdh. For further details and references on creeping waves the review by Gaunaurd (1989) can be consulted.

8. Concluding remarks

The scattering by an sdh has been considered by using the analytical solution. Realistic models of transmitting and receiving ultrasonic robes are used and the reception is in particular modelled with a reciprocity argument. To obtain simpler and more explicit and intuitive results the stationary phase

approximation is employed. However, it is noted that this approximation is often violated in practice and this is demonstrated with some numerical computations.

In practical NDT the sdh is used as a calibration reflector. The present developments are of course performed with this goal in mind and have in fact already been used for this purpose, see Boström and Wirdelius (1995) and Bövik and Boström (1997). These papers in fact report parts of a larger, still on-going, development of a computer code (called UTDefect) for the modelling of ultrasonic NDT in thick-walled components typical in the nuclear power industry, (Boström, 1995; Boström and Jansson, 1997, 2000). In this context it should also be noted that these developments give a validation of the present work as the scattering by a strip-like crack with the sdh as calibration has been favourably compared with experiments (Bövik and Boström, 1997; Boström, 1995: and Boström and Jansson, 2000).

Acknowledgement

The present work has been sponsored by the Swedish Nuclear Power Inspectorate (SKI) and this is gratefully acknowledged.

References

Auld, B.A., 1979. General electromechanical reciprocity relations applied to the calculation of elastic wave scattering coefficients. Wave Motion 1, 3–10.

Boström, A., 1995. UTDefect—a computer program modelling ultrasoic NDT of cracks and other defects. SKI Report 95:53 Swedish Nuclear Power Inspectorate, Stockholm.

Boström, A., Jansson, P.-Å., 1997. Development of UTDefect: rough cracks and probe arrays. SKI Report 97:28 Swedish Nuclear Power Inspectorate, Stockholm.

Boström, A., Jansson, P.-Å., 2000. Developments of UTDefect: rough rectangular cracks, anisotropy, etc. SKI Report 00:43 Swedish Nuclear Power Inspectorate, Stockholm.

Boström, A., Wirdelius, H., 1995. Ultrasonic probe modeling and nondestructive crack detection. J. Acoust. Soc. Am. 97, 2836–2848.

Bövik, P., Boström, A., 1997. A model of ultrasonic nondestructive testing for internal and subsurface cracks. J. Acoust. Soc. Am. 102, 2723–2733.

Chapman, R.K., 1990. A system approach for the ultrasonic inspection of smooth planar cracks. J. Nondestr. Eval. 9, 197–211.

Fellinger, P., Marklein, R., Langenberg, K.J., Klaholz, S., 1995. Numerical modeling of elastic wave propagation and scattering with EFIT—elastodynamic finite integration technique. Wave Motion 21, 47–66.

Gaunaurd, G.C., 1989. Elastic and acoustic resonance wave scattering. Appl. Mech. Rev. 42, 143–192.

Halkjaer, S., 2000. Elastic wave propagation in anisotropic, inhomogeneous materials—application to ultrasonic NDT. Thesis, Technical University of Denmark, Lyngby.

Harumi, K., Uchida, M., 1990. Computer simulation of ultrasonics and its applications. J. Nondestr. Eval. 9, 81–99.

Krautkrämer, J., Krautkrämer, H., 1990. Ultrasonic Testing of Materials, fourth ed. Springer, Berlin.

Olsson, S., 1994. Point force excitation of a thick-walled elastic infinite pipe with an embedded inhomogeneity. J. Engng. Math. 28, 311–325.

Pao, Y.-H., 1979. Betti's identity and transition matrix for elastic waves. J. Acoust. Soc. Am. 64, 302–310.

Pao, Y.-H., Mow, C.-C., 1973. Diffraction of Elastic Waves and Dynamic Stress Concentrations. Crane Russak, New York.

Schmerr, L.W., 1998. Fundamentals of Ultrasonic Nondestructive Evaluation: A Modelling Approach. Plenum, New York.

Varadan, V.V., Lakhtakia, A., Varadan, V.K., 1991. Field Representations and Introduction to Scattering. North-Holland, Amsterdam.

White, R.M., 1958. Elastic wave scattering at a cylindrical discontinuity in a solid. J. Acoust. Soc. Am. 30, 771–785.